Unified State-Feedback Control of a Hybrid Distribution Transformer using Particle Swarm Optimization Tuning

Dave Figueroa* dave.figueroa.dokt@pw.edu.pl
Alvaro Carreno* alvaro.carreno@pw.edu.pl
Mariusz Malinowski* malin@isep.pw.edu.pl
Liu Yang† yangliu_424@sina.com
Zhihong Zhao†‡ zhihongzhao@nbut.edu.cn

* Institute of Control and Industrial Electronics, Warsaw University of Technology, Warsaw, Poland.
† Research Institute of Interdisciplinary Intelligent Science, Ningbo University of Technology, Ningbo, China.
‡ Research Institute of Intelligent Control and Systems, Harbin Institute of Technology, Harbin, China.

***Abstract*—This paper presents a unified state-feedback control strategy for a hybrid distribution transformer (HDT) using particle swarm optimization (PSO) for tuning the control gains. The proposed control strategy aims to achieve zero steady-state error for sinusoidal references and disturbances while ensuring good dynamic performance. An augmented state-space model of the HDT is developed, incorporating delays from the digital control system and resonant states to ensure zero steady-state error. The control gains are optimized using PSO to minimize a cost function that considers both transient and steady-state performance. Simulation results demonstrate effectiveness of the proposed control strategy in regulating the voltage and current of the HDT under various operating conditions.**

***Index Terms*—Hybrid distribution transformer, optimal control, state-feedback control, particle swarm optimization**

I. Introduction

THE increasing penetration of renewable energy sources in the electrical grid has led to a significant rise in the use of power electronic converters. These converters are essential for integrating RES into the grid, as they facilitate the conversion of DC power generated by sources like solar panels and wind turbines into AC power compatible with the grid [1]. However, the widespread use of power electronic converters has also introduced challenges related to power quality, such as the injection of harmonics and non-linear loads, which can lead to voltage distortions and other issues in the electrical grid [2], [3].

There are many solutions that have been proposed to address the power quality issues in the grid, such as static compensators (STATCOMs) [4], dynamic voltage restorers (DVRs) [5], active power filters (APFs) [6], unified power quality conditioners (UPQCs) [7] and the solid-state transformers (SSTs) [8]. SSTs have the ability to mitigate most of the power quality issues mentioned above, while also providing galvanic isolation and voltage transformation. However, the high cost and complexity of SSTs have limited their widespread adoption in the distribution grid, and they also do not provide the same short-circuit current capability as traditional distribution transformers (DTs) [9].

For this reason, the hybrid distribution transformer (HDT) emerges as a promising solution to address the disadvantages of SSTs while still providing advanced power quality functionalities. The HDT is a power electronic transformer that combines the functions of a traditional distribution transformer with those of power electronic converters [10], [11]. Many HDT configurations have been proposed in the literature, and consequently, classifications have been proposed [9]. One of the classifications is based on the source of the converter's energy, i.e., whether the energy is obtained from a capacitor/battery, the primary or secondary side of the DT, or an auxiliary winding. On the other hand, the other classification is based on how the converters inject energy into the system, i.e., whether they are connected in series or in parallel with the DT.

Several control strategies have been proposed for the HDT in the literature, including finite control set model predictive control (FCS-MPC) [12], decoupled control strategies, such as the compound controller [13], quasi-proportional controller [14] and the separated multi-resonant state-feedback controller [15]. While these approaches have demonstrated good performance, they often rely on heuristic parameter tuning or treat the resonant compensation separately from the state-feedback framework, which complicates the design and limits systematic optimization.

In this paper, a unified control strategy based on state-feedback control is proposed for the HDT, where resonant states are incorporated only at a single natural frequency. This control strategy aims to achieve zero steady-state error for sinusoidal references and disturbances, while also ensuring good dynamic performance. The control strategy also considers the inherent delay present in real control microcontrollers. Moreover, instead of adjusting the feedback weights heuristically, as in conventional LQR designs, the proposed approach leverages particle swarm optimization (PSO) to automatically tune the control gains according to a cost function that balances transient and steady-state performance. This approach had been previously used for tuning the control gains for a VSI, achieving good results [16], [17]. The proposed control strategy is validated through simulation results that demonstrate its effectiveness in regulating the voltage and

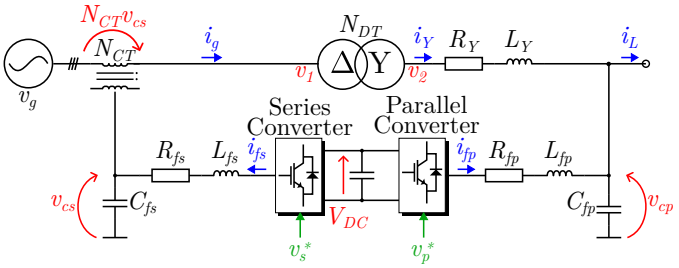

Fig. 1. Hybrid distribution transformer circuit diagram.

current of the HDT under various operating conditions.

II. Model of the Hybrid Distribution Transformer

The HDT configuration used in this paper is shown in Fig. 1. It consists of a traditional DT connected to two back-to-back VSCs: a series converter connected to the primary of the DT through a CT, and a parallel converter connected in parallel to the load, which is connected to the secondary of the DT. All the state-space equations are derived in the $\alpha\beta$ reference frame, until otherwise specified.

A. Series Converter

The objectives of the series converter are to compensate for voltage disturbances, e.g. sags, swells and harmonics that may occur in the grid. This is done by injecting a voltage in series with the grid through the CT. The dynamics of the series converter are given by the following state-space equation:

$$\dot{x}_s = \underbrace{\begin{bmatrix} -\frac{R_{fs}}{L_{fs}}\mathbf{I} & -\frac{1}{L_{fs}}\mathbf{I} \\ \frac{1}{C_{fs}}\mathbf{I} & \mathbf{0} \end{bmatrix}}_{\mathbf{A}_s} x_s + \underbrace{\begin{bmatrix} \frac{1}{L_{fs}}\mathbf{I} \\ \mathbf{0} \end{bmatrix}}_{\mathbf{B}_s} v_s + \underbrace{\begin{bmatrix} \mathbf{0} \\ -\frac{1}{C_{fs}}\mathbf{I} \end{bmatrix}}_{\mathbf{P}_{is}} i_s \quad (1)$$

where $x_s = \begin{bmatrix} i_{fs} & v_{cs} \end{bmatrix}^T$ is the state vector and i_s is the currents that circulates to the CT. The parameters R_{fs}, L_{fs}, and C_{fs} are the series converter filter resistance, inductance, and capacitance respectively.

The current i_s is related to the transformer secondary side current i_Y through $i_s = N_{CT} i_g$ relationship, where N_{CT} is the CT turns ratio and i_g is the grid current. The grid current can be expressed in terms of the transformer secondary side current and the parallel converter capacitor current as:

$$i_g^{abc} = \frac{1}{N_{DT}} \begin{bmatrix} 1 & 0 & -1 \\ -1 & 1 & 0 \\ 0 & -1 & 1 \end{bmatrix} i_Y^{abc} \quad (2)$$

where N_{DT} is the transformer turns ratio. Converting this to $\alpha\beta$ coordinates gives:

$$i_g = \frac{1}{N_{DT}} \mathbf{K}_{\mathbf{T}\alpha\beta}\, i_Y \quad (3)$$

where the matrix that models the $\Delta - Y$ transformer is given by:

$$\mathbf{K}_{\mathbf{T}\alpha\beta} = \begin{bmatrix} \frac{2}{3} & \frac{\sqrt{3}}{2} \\ -\frac{\sqrt{3}}{2} & \frac{3}{2} \end{bmatrix} \quad (4)$$

Substituting this into (1) gives:

$$\dot{x}_s = \mathbf{A}_s x_s + \mathbf{B}_s v_s + \mathbf{P}_{is} N_{CT} \frac{1}{N_{DT}} \mathbf{K}_{\mathbf{T}\alpha\beta}\, i_Y \quad (5)$$

B. Parallel Converter

The parallel converter is responsible for maintaining the dc-link voltage of the HDT and compensating load-side disturbances, including harmonics and unbalances that may be present. Its dynamics are expressed as:

$$\dot{x}_p = \underbrace{\begin{bmatrix} -\frac{R_{fp}}{L_{fp}}\mathbf{I} & -\frac{1}{L_{fp}}\mathbf{I} \\ \frac{1}{C_{fp}}\mathbf{I} & \mathbf{0} \end{bmatrix}}_{\mathbf{A}_p} x_p + \underbrace{\begin{bmatrix} \frac{1}{L_{fp}}\mathbf{I} \\ \mathbf{0} \end{bmatrix}}_{\mathbf{B}_p} v_p + \underbrace{\begin{bmatrix} \mathbf{0} \\ \frac{1}{C_{fp}}\mathbf{I} \end{bmatrix}}_{\mathbf{P}_{iY}} i_Y \quad (6)$$

$$+ \underbrace{\begin{bmatrix} \mathbf{0} \\ -\frac{1}{C_{fp}}\mathbf{I} \end{bmatrix}}_{\mathbf{P}_{iL}} i_L, \quad (7)$$

where $x_p = \begin{bmatrix} i_{fp} & v_{cp} \end{bmatrix}^T$ and i_L is the load current. The parameters R_{fp}, L_{fp}, and C_{fp} are the parallel converter filter resistance, inductance, and capacitance, respectively.

C. Transformer Dynamics

The secondary voltage of the transformer v_2 can be expressed in terms of the primary voltage v_1, given by $v_g + N_{CT} v_{cs}$, as:

$$v_2 = \frac{1}{N_{DT}} \mathbf{K}_{\mathbf{T}\alpha\beta}{}'(N_{CT} v_{cs} + v_g), \quad (8)$$

where $\mathbf{K}_{\mathbf{T}\alpha\beta}{}'$ is the transpose of the transformation matrix. The transformer dynamics, modeled as a series impedance referred to the Y side, are:

$$\dot{i_Y} = -\frac{R_Y}{L_Y} i_Y - \frac{1}{L_Y} v_{cp} + \frac{1}{L_Y} \frac{1}{N_{DT}} \mathbf{K}_{\mathbf{T}\alpha\beta}{}'(v_g + N_{CT} v_{cs}), \quad (9)$$

with R_Y and L_Y being the transformer series resistance and leakage inductance, respectively. The coupling matrices are

$$\mathbf{P}_{vg} = \frac{1}{L_Y} \frac{1}{N_{DT}} \mathbf{K}_{\mathbf{T}\alpha\beta}{}', \qquad \mathbf{P}_{vc} = \frac{1}{L_Y} \frac{N_{CT}}{N_{DT}} \mathbf{K}_{\mathbf{T}\alpha\beta}{}'.$$

D. Overall HDT Model

By combining the series converter, parallel converter, and transformer dynamics, the overall state-space model of the HDT can be compactly expressed as:

$$\begin{bmatrix} \dot{x}_s \\ \dot{x}_p \\ \dot{i_Y} \end{bmatrix} = \underbrace{\begin{bmatrix} \mathbf{A}_s & \mathbf{0} & \mathbf{0} \\ \mathbf{0} & \mathbf{A}_p & \mathbf{P}_{iY} \\ \mathbf{P}_{vc}\mathbf{M} & -\frac{1}{L_Y}\mathbf{M} & -\frac{R_Y}{L_Y}\mathbf{I} \end{bmatrix}}_{\mathbf{A}} \begin{bmatrix} x_s \\ x_p \\ i_Y \end{bmatrix}$$

$$+ \underbrace{\begin{bmatrix} \mathbf{B}_s & \mathbf{0} \\ \mathbf{0} & \mathbf{B}_p \\ \mathbf{0} & \mathbf{0} \end{bmatrix}}_{\mathbf{B}} \begin{bmatrix} v_s \\ v_p \end{bmatrix} + \underbrace{\begin{bmatrix} \mathbf{0} & \mathbf{0} \\ \mathbf{0} & \mathbf{P}_{iL} \\ \mathbf{P}_{vg} & \mathbf{0} \end{bmatrix}}_{\mathbf{P}} \begin{bmatrix} v_g \\ i_L \end{bmatrix},$$

with the overall state vector $x = \begin{bmatrix} x_s^T & x_p^T & i_Y^T \end{bmatrix}^T$, disturbance vector $d = \begin{bmatrix} v_g & i_L \end{bmatrix}$ and input vector $u_k = \begin{bmatrix} v_s^T & v_p^T \end{bmatrix}^T$. The selection matrix $\mathbf{M} = \begin{bmatrix} \mathbf{0} & \mathbf{I} \end{bmatrix}$ extract the capacitor voltages

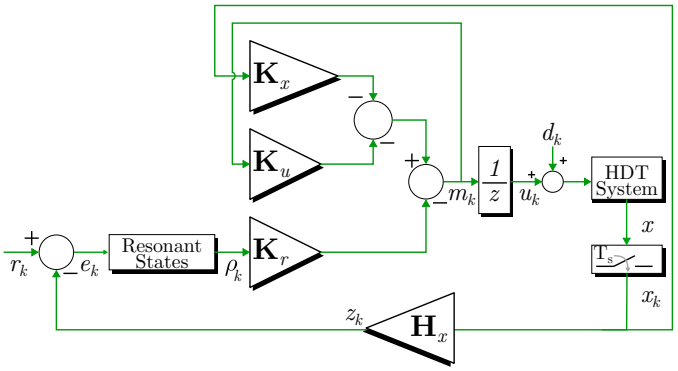

Fig. 2. Block diagram of the proposed control strategy for the HDT.

v_{cp} and v_{cs} from the parallel and series converter states, respectively.

The HDT system is discretized using a zero-order hold which gives the following state-space model:

$$\begin{aligned} x_{k+1} &= \mathbf{A}_d x_k + \mathbf{B}_d u_k + \mathbf{P}_d d_k \\ y_k &= \mathbf{C} x_k \end{aligned} \tag{10}$$

where $\mathbf{A}_d = e^{\mathbf{A}T_s}$, $\mathbf{B}_d = \int_0^{T_s} e^{\mathbf{A}\tau} d\tau \mathbf{B}$, $\mathbf{P}_d = \int_0^{T_s} e^{\mathbf{A}\tau} d\tau \mathbf{P}$, and $\mathbf{C} = \mathbb{I}$.

In most of the applications, there is a delay of one sampling period between the calculation of the control input and its application to the system. To account for this delay, the discrete-time state-space model is augmented with a new state representing the previous control input:

$$u_{k+1} = m_k \tag{11}$$

This can be expressed in state-space form as:

$$\begin{bmatrix} x_{k+1} \\ u_{k+1} \end{bmatrix} = \underbrace{\begin{bmatrix} \mathbf{A}_d & \mathbf{B}_d \\ \mathbf{0} & \mathbf{0} \end{bmatrix}}_{\mathbf{A}_{d,\text{delay}}} \begin{bmatrix} x_k \\ u_k \end{bmatrix} + \underbrace{\begin{bmatrix} \mathbf{0} \\ \mathbf{I} \end{bmatrix}}_{\mathbf{B}_{d,\text{delay}}} m_k \tag{12}$$

where $\mathbf{A}_{d,\text{delay}}$ and $\mathbf{B}_{d,\text{delay}}$ are the augmented system and input matrices respectively.

III. Control Strategy

With the state-space model of the HDT defined, the next step is to design a control strategy that ensures the desired performance.

A. Proposed Control Strategy

The proposed control strategy is based on a state-feedback controller which is designed using the augmented state-space model of the HDT, defined in (12). The control strategy aims to achieve zero steady-state error for sinusoidal references. To achieve this, the system is expanded with the following resonant terms:

$$\dot{\rho}_1 = \underbrace{\begin{bmatrix} 0 & \omega \\ -\omega & 0 \end{bmatrix}}_{\mathbf{A}_{r1}} \rho_1 + \underbrace{\begin{bmatrix} 1 \\ 0 \end{bmatrix}}_{\mathbf{B}_{r1}} e_1 \tag{13}$$

where ω is the nominal angular frequency, ρ_1 and e are the first resonant and error components respectively. Each reference signal has two associated resonant states. Therefore, HDT control requires eight resonant states in total (four for $ev_{cs,\alpha\beta}$ and four for $i_{fp,\alpha\beta}$). This can be expressed as:

$$\begin{aligned} \dot{\rho} = &\underbrace{\text{diag}(\mathbf{A}_{r1}, \mathbf{A}_{r1}\mathbf{A}_{r1}, \mathbf{A}_{r1})}_{\mathbf{A}_r} \rho \\ &+ \underbrace{\text{diag}(\mathbf{B}_{r1}, \mathbf{B}_{r1}, \mathbf{B}_{r1}, \mathbf{B}_{r1})}_{\mathbf{B}_r} e \end{aligned} \tag{14}$$

These resonant states are then discretized using a ZOH giving the matrices $\mathbf{A}_{rd}$ and $\mathbf{B}_{rd}$. Hence, the expanded system that includes the augmented state-space defined in (12) and the resonant terms defined in (14) is defined as:

$$\begin{aligned} \begin{bmatrix} x_{k+1} \\ u_{k+1} \\ \rho_{k+1} \end{bmatrix} &= \underbrace{\begin{bmatrix} \mathbf{A}_{d,delay} & \mathbf{0} \\ \mathbf{B}_{rd}\mathbf{H}_x & \mathbf{A}_{rd} \end{bmatrix}}_{\mathbf{A}_{d,\text{aug}}} \begin{bmatrix} x_k \\ u_k \\ \rho_k \end{bmatrix} + \underbrace{\begin{bmatrix} \mathbf{B}_{d,\text{delay}} \\ \mathbf{0} \end{bmatrix}}_{\mathbf{B}_{d,\text{aug}}} \begin{bmatrix} m_k \\ r_k \end{bmatrix} \\ y_k &= \begin{bmatrix} \mathbf{C} & \mathbf{0} \end{bmatrix} \begin{bmatrix} x_k \\ u_k \\ \rho_k \end{bmatrix}, \quad e_k = r_k - \mathbf{H}_x x_k \end{aligned} \tag{15}$$

where the matrix $\mathbf{H}_x$ selects the states with reference following and r_k is the reference vector. Then, the state-feedback controller is designed using the discrete LQR approach given by:

$$\mathbf{K} = \text{dlqr}(\mathbf{A}_{d,\text{aug}}, \mathbf{B}_{d,\text{aug}}, \mathbf{Q}, \mathbf{R}) \tag{16}$$

where $\mathbf{Q} \in \mathbb{R}^{11}$ and $\mathbf{R} \in \mathbb{R}^4 = \mathbf{I}$ are the state and input weighting matrices, respectively. The gain matrix is partitioned into three sub-matrices: $\mathbf{K}_x$, $\mathbf{K}_u$ and $\mathbf{K}_r$ for convenience. The block diagram of the proposed control strategy is shown in Fig. 2. With the partitioned gain matrices defined, the control input can be expressed as:

$$m_k = -\mathbf{K}_x x_k - \mathbf{K}_u u_k - \mathbf{K}_r \rho_k \tag{17}$$

where $\mathbf{K}_x$ is the state-feedback gain matrix, $\mathbf{K}_u$ is the previous control input gain matrix and $\mathbf{K}_r$ is the resonant states gain matrix.

The series converter reference is calculated as the difference between the nominal value of the grid voltage and the actual value and the parallel converter reference is the sum of the DC-link control loop, which uses the instantaneous power theory [18], and the harmonic elimination control loop. This is based on the work of Carreno et al. [15].

B. Particle Swarm Optimization

To facilitate the tuning of the state-feedback gain matrix $\mathbf{K}$ by adjusting $\mathbf{Q}$, the PSO algorithm is employed to optimize the weights associated with each state in the cost function. The PSO algorithm is a population-based optimization technique inspired by the social behavior of birds and fish [19]. It consists of a swarm of particles, where each particle represents a potential solution to the optimization problem, in this case, the vector of powers $q_{x,j}(i)$, where x, j and i are the state, particle and iteration numbers. The particles move through the search space, updating their positions based on their own experience and the experience of their neighbors. The velocity

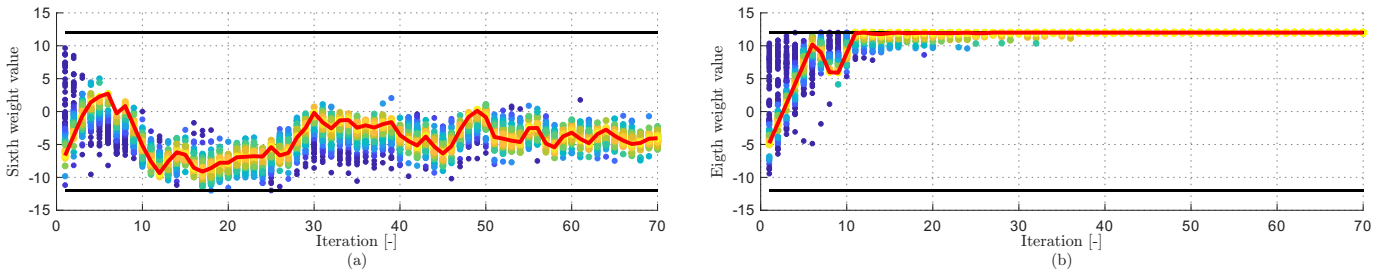

Fig. 3. Convergence of exponents over the PSO iterations. (a) Exponent q_6 associated with the parallel converter inductor current $v_{cp,\alpha\beta}$. (b) Exponent q_8 associated with the first resonant state of the error $e1v_{cs,\alpha\beta}$.

and position of each particle are updated using the following equations:

$$\begin{aligned} v_j(i+1) &= K_{ap}\left(v_j(i) + c_1 r_1(pbest_j - x_j(i))\right. \\ &\quad \left. + c_2 r_2(gbest - x_j(i))\right) \\ x_j(i+1) &= x_j(i) + v_j(i+1) \end{aligned} \tag{18}$$

where $v_j(i)$, $x_j(i)$, $pbest_j$ and $gbest$ are the velocity, position, the best position and global-best position of the particle j at iteration i. c_1 and c_2 are cognitive and social acceleration coefficients, r_1 and r_2 are random numbers uniformly distributed in the range [0, 1], and K_{ap} is the constriction factor given by:

$$K_{ap} = \frac{2}{\left|2 - \phi - \sqrt{\phi^2 - 4\phi}\right|} \tag{19}$$

where $\phi = c_1 + c_2 > 4$ is a constant that ensures convergence.

The PSO algorithm iteratively updates the positions and velocities of the particles until the maximum number of iterations is reached. The best position found by the swarm is considered the optimal solution to the optimization problem.

C. PSO Performance Index

The performance index used for the PSO optimization is a cost function that considers both the transient and steady-state performance of the HDT [16]. This index is minimized through many iterations considering the HDT system with step of sinusoidal references and without any applied disturbances. The cost function is defined as:

$$J = \frac{1}{N}\sum_{i=1}^{N} |e_k|^2 + \beta \Delta u_k^2 \tag{20}$$

where N is the number of samples in the simulation, Δu_k is the change in control input at sample k, and β is a weighting factor that balances the importance of the transient and steady-state performance, which is the only parameter that should be tuned according to the simulation results from the iterations process.

The assumptions made when running the PSO algorithm are that the penalties for the α and β components are equal, including the resonant terms for each of the components. For that reason, the search of space is reduced from 22 states to half. Also, to simplify the search space of the swarm, the particles are represented as exponents of the state weights. This can be expressed as:

$$\mathbf{Q} = \text{diag}\left\{10^{q_1}\mathbf{I}, 10^{q_2}\mathbf{I}, ..., 10^{q_{11}}\mathbf{I}\right\} \tag{21}$$

TABLE I
PSO PARAMETERS USED FOR THE OPTIMIZATION OF THE CONTROL GAINS.

Parameter	Value
Number of particles	100
Maximum number of iterations	70
Maximum weight exponent for states	$[-20, 20]$
Absorbing walls boundaries	$[-12, 12]$
Cognitive acceleration coefficients (c_1, c_2)	2.05
Performance index weighting factor (β)	2×10^{-7}

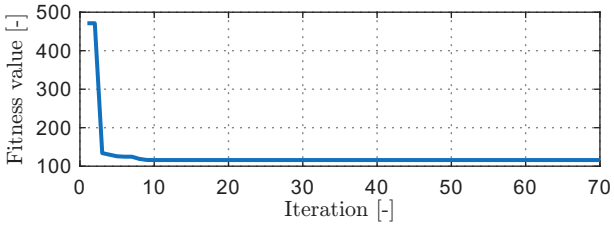

Fig. 4. Convergence of the fitness value over the PSO iterations.

The optimization variables lie within a defined range including the absorbing walls boundaries [20] which allows obtaining a not-large LQR gain. The PSO parameters used for the optimization are listed in Table I.

TABLE II
OPTIMIZED STATE WEIGHT EXPONENTS q_i FROM PSO.

q_1	q_2	q_3	q_4	q_5	q_6
-6.186	-7.810	-4.406	-1.642	-8.674	-5.315
q_7	q_8	q_9	q_{10}	q_{11}	
-11.118	11.999	9.672	10.516	8.827	

After running the PSO algorithm, each of the optimal state weights exponents (q_x) that the algorithm found are given in the Table II. As an example, the convergence of two of the exponents over the PSO iterations is shown in Fig. 3, while the convergence of the fitness value over the PSO iterations is shown in Fig. 4.

IV. Simulation Results

In this section, the simulation results of the proposed control strategy are presented. The simulations are performed using MATLAB/Simulink, and the system parameters are listed in Table III. The proposed control strategy is tested under grid

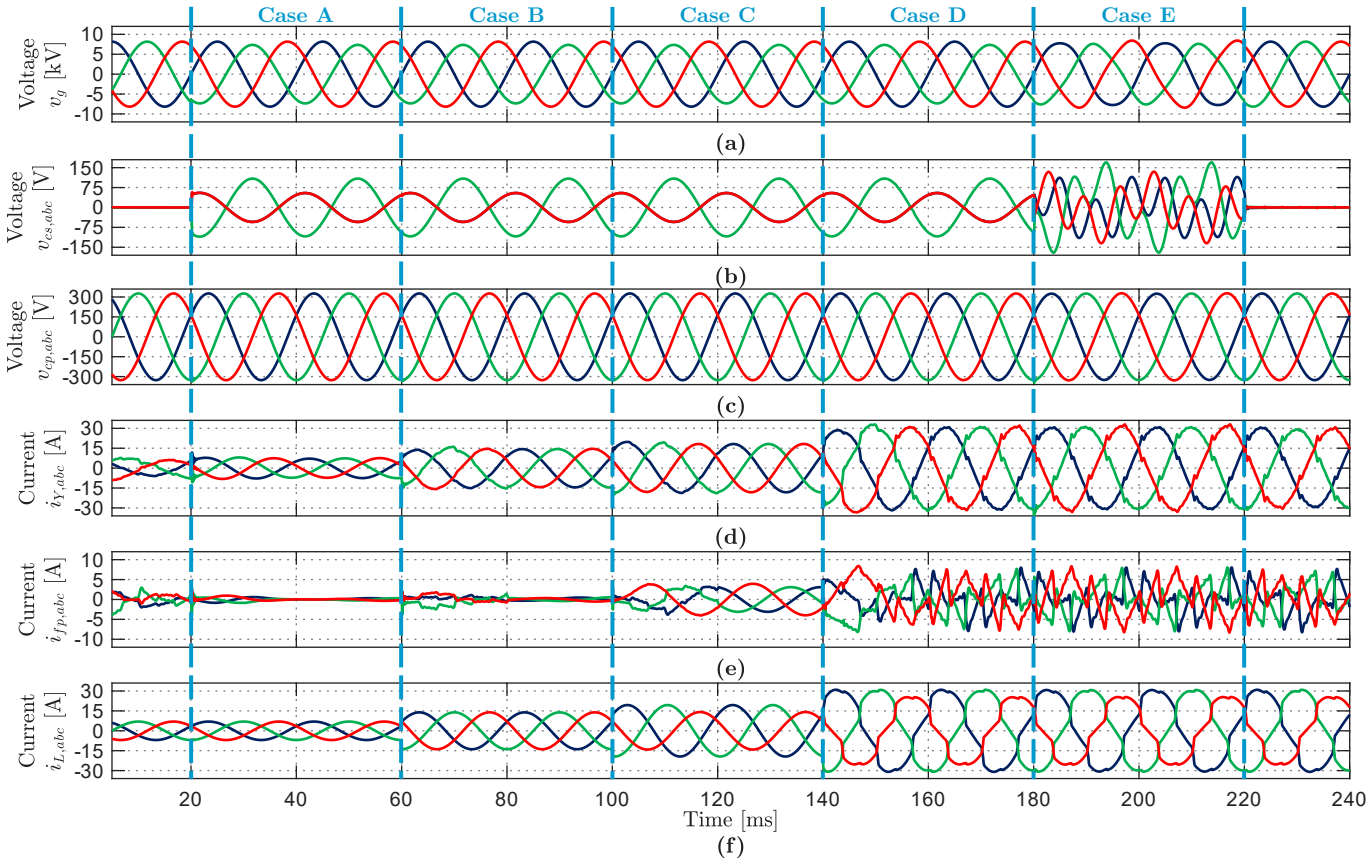

Fig. 5. Simulation results in *abc* coordinates for the proposed control strategy under grid and load disturbances. (a) Grid voltage, (b) Series converter output voltage, (c) Parallel converter output voltage, (d) Secondary side transformer current, (e) Parallel converter current, (f) Load current

unbalanced swell, load impact, load unbalance, and non-linear load conditions.

TABLE III
SYSTEM PARAMETERS

Parameter	Variable	Value
Grid Voltage	V_g	10 kV
Nominal Converter Voltage	V_s	400 V
DC Link Voltage	V_{DC}	700 V
Grid Frequency	f_e	50 Hz
Series Converter Filter Inductance	L_{fs}	200 μH
Series Converter Filter Resistance	R_{fs}	100 mΩ
Series Converter Filter Capacitance	C_{fs}	12 μF
Parallel Converter Filter Inductance	L_{fp}	200 μH
Parallel Converter Filter Resistance	R_{fp}	100 mΩ
Parallel Converter Filter Capacitance	C_{fp}	12 μF
Transformer Dispersion Inductance	L_Y	100 μH
Transformer Series Resistance	R_Y	5 mΩ
Coupling Transformer Turns Ratio	N_{CT}	5
Distribution Transformer Turns Ratio	N_{DT}	$V_s/(V_g\sqrt{3})$
Converters Switching Frequency	f_{sw}	20 kHz
Control Sampling Time	T_s	50 µs

A. Grid Voltage Unbalanced Swell Compensation

From the instant $t = 20\ ms$ until $t = 220\ ms$, a three-phase unbalanced swell of 10% the nominal value, in phase b is applied to the grid voltage, as shown in Fig. 5.(a). The nominal balanced resistive load of 47 Ω is connected to the HDT. The proposed control strategy effectively compensates for the unbalanced swell, meaning that the parallel inverter injects the necessary voltage to maintain a balanced transformer secondary side current, as shown in Fig. 5.(d).

B. Load Impact

At $t = 60\ ms$, a three-phase balanced load impact of 47 Ω per phase is applied, as shown in Fig. 5.(b). In this case, the parallel converter supplies the needed current to provide additional power so the DC-link voltage will be balanced.

C. Unbalanced Load Compensation

Following the load impacts, at $t = 100\ ms$ an unbalanced load of 94 Ω between b and c is connected in parallel to the existing loads. The parallel converter injects the necessary current to maintain a balanced transformer secondary side current, as shown in Fig. 5.(e). Therefore, the control strategy manages to keep i_Y with balanced magnitudes, as is obtained in Fig. 5.(f)

D. Non-linear Load Compensation

At $t = 140\ ms$, a three-phase diode bridge rectifier with a 47 Ω resistive load at its output is applied, as shown in Fig. 5.(f). In this case, additionally to the existing DC-link control, the reference is calculated by the actuation of the harmonics compensation control loop, which compensates the harmonics that the non-linear load injects to the secondary side, which can be seen in the Fig. 5.(f). The proposed control

strategy manages to compensate this disturbance, maintaining the transformer secondary side current sinusoidal and balanced, as shown in Fig. 5.(d).

E. Grid Voltage 3rd Harmonic Distortion

Finally, at $t = 180\ ms$, a third harmonic component is added to the grid voltage, as shown in Fig. 5.(a). In this case, the series converter reference is composed by the grid voltage harmonics plus the existing voltage swell compensation, as illustrated in Fig. 5.(b). The proposed control strategy effectively compensates for this disturbance, maintaining a clean transformer secondary side current sinusoidal and balanced, as shown in Fig. 5.(d).

V. Conclusions

In the present paper a unified state-feedback control strategy for a HDT was proposed. The control strategy was designed using an augmented state-space model of the HDT that includes the delays introduced by the digital control system and resonant states to achieve zero steady-state error for sinusoidal references. The control gains were optimized using PSO to minimize a cost function that considers both the transient and steady-state performance of the HDT. This enables optimal weight selection during the state-feedback controller tuning instead of relying on heuristic or trial-and-error tuning.

The proposed control strategy was validated through simulation results that demonstrated its effectiveness in regulating the voltage and current of the HDT under various operating conditions, including grid voltage unbalanced swell compensation, load impact and unbalanced load compensation, nonlinear load compensation, and grid harmonics compensation.

VI. Acknowledgments

This work was supported by the National Science Centre (NCN), Poland, under grant UMO-2024/55/B/ST7/00208.

References

[1] F. Blaabjerg, Y. Yang, K. A. Kim, and J. Rodriguez, "Power electronics technology for large-scale renewable energy generation," *Proceedings of the IEEE*, vol. 111, no. 4, pp. 335–355, 2023.

[2] M. Najafzadeh, R. Ahmadiahangar, O. Husev, I. Roasto, T. Jalakas, and A. Blinov, "Recent contributions, future prospects and limitations of interlinking converter control in hybrid ac/dc microgrids," *IEEE Access*, vol. 9, pp. 7960–7984, 2021.

[3] S. Sepasi, C. Talichet, and A. S. Pramanik, "Power quality in microgrids: A critical review of fundamentals, standards, and case studies," *IEEE Access*, vol. 11, pp. 108 493–108 531, 2023.

[4] T. Engelbrecht, A. Isaacs, S. Kynev, J. Matevosyan, B. Niemann, A. J. Owens, B. Singh, and A. Grondona, "Statcom technology evolution for tomorrow's grid: E-statcom, statcom with supercapacitor-based active power capability," *IEEE Power and Energy Magazine*, vol. 21, no. 2, pp. 30–39, 2023.

[5] T. Kandil and M. Adel Ahmed, "Control and operation of dynamic voltage restorer with online regulated dc-link capacitor in microgrid system," *Canadian Journal of Electrical and Computer Engineering*, vol. 43, no. 4, pp. 331–341, 2020.

[6] A. K. Mishra, S. R. Das, P. K. Ray, R. K. Mallick, A. Mohanty, and D. K. Mishra, "Pso-gwo optimized fractional order pid based hybrid shunt active power filter for power quality improvements," *IEEE Access*, vol. 8, pp. 74 497–74 512, 2020.

[7] H. Fujita and H. Akagi, "The unified power quality conditioner: the integration of series- and shunt-active filters," *IEEE Transactions on Power Electronics*, vol. 13, no. 2, pp. 315–322, 1998.

[8] J. E. Huber and J. W. Kolar, "Applicability of solid-state transformers in today's and future distribution grids," *IEEE Transactions on Smart Grid*, vol. 10, no. 1, pp. 317–326, 2019.

[9] A. Carreno, M. Perez, C. Baier, A. Huang, S. Rajendran, and M. Malinowski, "Configurations, Power Topologies and Applications of Hybrid Distribution Transformers," *Energies*, vol. 14, no. 5, p. 1215, Feb. 2021.

[10] M. Y. Haj-Maharsi, L. Tang, R. Gutierrez, and S. Bala, "Hybrid distribution transformer with ac & dc power capabilities," US Patent US20 100 201 338A1, Aug., 2010.

[11] W. Matelski, "Badania eksperymentalne transformatora hybrydowego jako kondycjonera napięcia w sieciach typu TN," *PRZEGLĄD ELEKTROTECHNICZNY*, vol. 1, no. 5, pp. 233–238, May 2023.

[12] P. Costa, G. Paraíso, S. F. Pinto, and J. F. Silva, "A four-leg matrix converter based hybrid distribution transformer for smart and resilient grids," *Electric Power Systems Research*, vol. 203, p. 107650, Feb. 2022.

[13] Y. Liu, D. Liang, P. Kou, M. Zhang, S. Cai, K. Zhou, Y. Liang, Q. Chen, and C. Yang, "Compound Control System of Hybrid Distribution Transformer," *IEEE Transactions on Industry Applications*, vol. 56, no. 6, pp. 6360–6373, Nov. 2020.

[14] Y. Liu, L. Zhang, D. Liang, H. Jin, S. Li, S. Jia, J. Li, H. Liu, Y. Wang, K. Zhou, Y. Gao, S. Cai, D. Li, and S. Feng, "Quasi-Proportional-Resonant Control for the Hybrid Distribution Transformer With LCL-Type Converters," *IEEE Transactions on Industry Applications*, vol. 58, no. 5, pp. 6368–6385, Sep. 2022.

[15] A. Carreno, M. A. Perez, and M. Malinowski, "State-Feedback Control of a Hybrid Distribution Transformer for Power Quality Improvement of a Distribution Grid," *IEEE Transactions on Industrial Electronics*, vol. 71, no. 2, pp. 1147–1157, Feb. 2024.

[16] B. Ufnalski, A. Kaszewski, and L. M. Grzesiak, "Particle Swarm Optimization of the Multioscillatory LQR for a Three-Phase Four-Wire Voltage-Source Inverter With an LC Output Filter," *IEEE Transactions on Industrial Electronics*, vol. 62, no. 1, pp. 484–493, Jan. 2015.

[17] A. Galcki, M. Michalczuk, B. Ufnalski, and L. M. Grzesiak, "Particle Swarm Optimization of the State Feedback Current Controller with Oscillatory Terms for a Three-Phase Grid-Tie Converter," in *2018 20th European Conference on Power Electronics and Applications (EPE'18 ECCE Europe)*, Sep. 2018, pp. P.1–P.10.

[18] H. Akagi, A. Nabae, and S. Atoh, "Control Strategy of Active Power Filters Using Multiple Voltage-Source PWM Converters," *IEEE Transactions on Industry Applications*, vol. IA-22, no. 3, pp. 460–465, May 1986.

[19] M. Clerc, "The swarm and the queen: Towards a deterministic and adaptive particle swarm optimization," in *Proceedings of the 1999 Congress on Evolutionary Computation-CEC99 (Cat. No. 99TH8406)*, vol. 3, Jul. 1999, pp. 1951–1957 Vol. 3.

[20] J. Robinson and Y. Rahmat-Samii, "Particle swarm optimization in electromagnetics," *IEEE Transactions on Antennas and Propagation*, vol. 52, no. 2, pp. 397–407, Feb. 2004.